A Sustainable and Low-Cost Zn-Lignosulfonate Redox Flow Battery

Athul Seshadri Ramanujam, Paula Navalpotro, Nagaraj Patil,* and Rebeca Marcilla*

Aqueous organic redox flow batteries offer great promise for long-duration stationary energy storage but are often hindered by high costs associated with synthetic redox-active materials and expensive ion-exchange membranes. Polymer-based redox species allow the use of cheaper microporous membranes, yet synthetic redox polymers remain costly to produce. In this study, a cost-effective zinc/lignosulfonate hybrid redox flow battery (RFB) is presented, employing commercial sodium lignosulfonate (NaLS) as a biopolymer catholyte, Zn foil as a low-cost and abundant anode, and a cost-effective size-exclusion cellulose membrane as the separator. The sluggish electrochemical behavior of the NaLS is enhanced by using carbon-impregnated felt electrodes. Using 10 mM NaLS (20 kDa), the system achieves an average discharge voltage of 0.98 V and an initial capacity of 1.41 Ah L^{-1} (9.4 mAh g^{-1}), outperforming previous lignin-based RFBs. Increasing NaLS concentration to 30 mM boosts capacity to 3.52 Ah L^{-1}, although the cycling stability in 1 M ZnSO$_4$ remain moderate. However, increasing the ZnSO$_4$ concentration to 3 M further improves cyclability, with capacity retention rising to 72% over 28 days, compared to 66% over 17 days for 1 M ZnSO$_4$. This work represents the first demonstration of commercial lignosulfonate as a catholyte in Zn-hybrid RFBs, showcasing its potential as a sustainable active material with a remarkably low electrolyte cost of 26 € kWh^{-1}.

1. Introduction

With the global emphasis on achieving carbon neutrality or "net-zero" emissions, advancements in renewable energy are poised to play a critical role in the energy transition.[1] The International Energy Agency (IEA) identifies renewable energy as a key driver for achieving global net-zero emissions by 2050.[2] However, the intermittent nature of two major renewable energy sources—solar and wind, presents significant challenges for grid stability.[3] Large-capacity, long-duration energy storage solutions are essential to buffer these fluctuations and ensure the reliable integration of renewables into the grid.[4] Redox flow batteries (RFBs) offer a promising solution for grid-scale energy storage due to their modular design, which decouples energy storage capacity from power output, making them particularly suitable for long-duration applications.[5,6] Among various RFB chemistries,

vanadium redox flow batteries (VRFBs) currently dominate the market owing to their high cycling stability and scalability.[7–9] However, the necessary use of expensive ion-selective separators such as Nafion, the high cost and criticality of vanadium, and environmental concerns associated with its mining and disposal, have limited their broader commercialization.[10–12]

In the last years, aqueous organic redox flow batteries (AORFBs), based on organic redox-active materials, have emerged as a compelling alternative. They mitigate some of these issues by utilizing cost-effective, abundant, and environmentally benign organic materials,[13–15] including small molecules, polymers, nanogels, and colloids, all exhibiting attractive electrochemical properties.[16–18] Furthermore, organic redox molecules offer exceptional tunability in redox potential, solubility, stability, and conductivity, enabled through macromolecular engineering.[19]

Redox-active polymers are particularly appealing for AORFB because they allow the use of microporous membranes, which are significantly less expensive, only 5–10% of the cost of conventional Nafion.[20,21] In fact, their hydrodynamic radii, can be precisely controlled to minimize crossover of active species while still enabling the migration of smaller ions as charge carriers, thus facilitating the use of cost-effective microporous separators.[22,23] Schubert et al. introduced the first all-polymer aqueous RFB, employing viologen-based and 2,2,6,6-tetramethyl-1-piperidinyloxy (TEMPO)-based redox-active polymers as the anolyte and catholyte, respectively, and where Nafion was substituted by cellulose-based dialysis membrane.[24] This first system exhibited a volumetric capacity of 8.7 Ah L^{-1}, with 75% capacity retention over 100 cycles. Subsequent improvements in the solubility of poly(TEMPO) by employing zwitterionic sulfopropylammonium copolymer segments, resulted in capacities exceeding

A. S. Ramanujam, P. Navalpotro, N. Patil, R. Marcilla
Electrochemical Processes Unit
IMDEA Energy
Avda., Ramón de la Sagra 3, 28935 Móstoles, Spain
E-mail: nagaraj.patil@imdea.org
         rebeca.marcilla@imdea.org

A. S. Ramanujam
Department of Applied Chemistry, Faculty of Chemistry
University of the Basque Country (UPV/EHU)
Avda., Manuel de Lardizabal 3, 20018 Donostia-San Sebastián, Spain

Batteries & Supercaps

Research Article
doi.org/10.1002/batt.202500529

Chemistry
Europe
European Chemical
Societies Publishing

20 Ah L^{-1}.[25] Kumar and Tripathi reported a similar viologen-based polymer as negolyte and a ferrocene-based polymer as catholyte, obtaining a AORFB with 0.85 V and a reasonable cycling stability (82% capacity retention after 250 cycles at 10 mA cm^{-2}), albeit with a modest capacity (3.02 Ah L^{-1}).[23]

Unlike classical RFBs that use soluble redox-active species, Yan et al. developed an all-polymer RFB with a poly(hydroquinone)/poly(imide) slurry-based particulate system, achieving a discharge capacity of 4.95 Ah L^{-1}.[26] Hatakeyama-Sato et al. extended this approach to design various nanoparticle-based polymer electrolytes, achieving higher cell voltages (1.1 and 1.3 V) and enhanced redox kinetics.[22] Both examples highlight the potential of expanding the range of viable redox-active polymers beyond traditional soluble species when using redox suspensions. Overall these studies highlight the versatility of synthetic polymers as highly effective redox-active materials for RFBs, however their production remains complex, environmentally taxing, and commercially unviable without cost-effective manufacturing methods.[27,28]

To address the challenges of purely organic systems, metal–organic hybrid RFBs have been proposed. These systems pair an organic catholyte with a metallic anode, thereby combining the advantages of both components—namely, the cost-effectiveness and tunability of organic catholytes and the high gravimetric capacity and low redox potential of metal anodes.[29] Over the past decade hybrid organic RFBs based on lithium (Li), magnesium (Mg), and zinc (Zn) have been developed.[30–32] Among these metallic anodes, Zn stands out due to its high volumetric capacity (5.85 Ah mL^{-1}), and favorable compatibility with aqueous electrolytes, attributed to its moderately negative standard electrode potential (−0.76 V vs. standard hydrogen electrode (SHE)). Additionally, zinc is abundant, cost-effective, and widely available, making its combination with organic-based catholyte a particularly promising strategy for the development of sustainable and scalable battery technologies.

While most Zn/organic RFBs developed to date rely on soluble small molecules as redox-active species, they require expensive ion-selective membranes to prevent active species crossover, contributing significantly to system cost. Efforts to employ soluble synthetic redox polymers, as outlined below, which enable the use of size-exclusion membranes (SEM), have shown promise but are typically limited to lab-scale materials obtained through complex multistep synthesis and purification routes.

Zhao et al. proposed a Zn-hybrid RFB using a polyaniline (PANI) suspension as the catholyte. This system, featuring a single-flow design with a polypropylene microporous membrane, demonstrated a high initial capacity of 17.3 Ah L^{-1}. However, it suffered from poor cycling stability, with a fast capacity decay of 0.07% per cycle over 32 cycles at 20 mA cm^{-2}, along with a relatively low average coulombic efficiency (CE) of 86%.[33] Similarly, Fernandez-Benito et al. employed amphiphilic block copolymer nanoparticles functionalized with redox-active ferrocene units as the catholyte dispersion. However, the resultant Zn-hybrid RFB perform poorly, operating at an impractically low current (0.027 mA) and achieving a very low capacity (124 mAh L^{-1}, corresponding to 1.9 mM concentration).[34]

Additionally, severe capacity fade within only 10 cycles, attributed to nanoparticle aggregation and sedimentation, further questioned the system's stability and feasibility. Volodin et al. examined the thermal stability of another ferrocene-based copolymer (PFc) used as a catholyte in a Zn-hybrid RFB. The RFB delivered an initial capacity of 0.76 Ah L^{-1}.[35] In their optimized thermostat setup, the capacity fade rate remained at 0.2% d^{-1} up to 38 °C, increased to 0.2% d^{-1} at 50 °C, and accelerated significantly at 60 °C. Ultimately, research specifically targeting Zn/polymer AORFBs remains very limited, with most examples showing low capacities and significant capacity decay. Moreover, in all these examples, the redox-active polymers employed are synthetic materials obtained through multistep, complex, and costly synthetic routes. These factors restrict their scalability and commercial viability. In contrast, natural biopolymers such as lignin offer a low-cost and renewable alternative with potential compatibility with inexpensive microporous membranes.

Lignin, an abundant byproduct of the pulp and paper industry, represents a sustainable and cost-effective alternative to synthetic polymers, with annual production projected to exceed 225 million tons by 2030.[36] Rich in redox-active phenolic and quinone groups, lignin is nontoxic, abundant, and inexpensive biopolymer.[37,38] Among technical lignins, lignosulfonate (LSs) holds the largest market share[39] offering aqueous solubility, structural flexibility, and commercial availability.[40,41] Owing to these properties, LSs have already been explored as active materials in RFBs. However, the main challenge with lignin is its poor electrochemical reversibility that is affected by factors such as the type of monolignol groups in the lignin, nature of cationic charge carriers, and the pH of the electrolyte.[42–44] Mukhopadhyay et al., pioneered the development of lignin-based RFB pairing ultrafiltered LSs (0.1 M LS in 0.1 M HClO$_4$) as acidic negolyte with Br$_2$/HBr catholyte.[45] Although feasible, the low cell discharge voltage (≈0.15 V) and low capacity (0.3 Ah L^{-1} at 10 mA cm^{-2}) significantly limited its practical application. Subsequently, Schlemmer et al. employed deformylated vanillin as the catholyte active material, leveraging vanillin's availability as a commercially produced lignin-derived fine chemical. As in the preceding study, an acidic electrolyte comprising 0.5 M H$_3$PO$_4$ was used. The resulting RFB delivered a capacity of ≈112 mAh L^{-1} and exhibited a capacity retention of 87.4% over 250 cycles.[46] A few lignin-based alkaline RFBs were reported by Jiao et al., who investigated two lignin monomers—coniferaldehyde (G) and sinapaldehyde (S), as well as an anthraquinone-modified lignin as active materials, paired with K$_4$[Fe(CN)$_6$] in 1 M KOH.[47,48] However, the resulting RFB exhibited very low specific capacities (≈100−150 mAh g^{-1}) during potentiostatic cycling at ±0.5 V, denoting their significant limitations in effective energy storage. In a recent study, Chakraborty et al. successfully modified the structure of soda-based lignin by oxidative depolymerization achieving modified lignin compound with improved electrochemical activity and reversibility. This depolymerized lignin was employed as anolyte paired with K$_4$[Fe(CN)$_6$] anolyte in an alkaline RFB but its performance remained limited, achieving a maximun capacity of 84.2 mAh L^{-1} and a capacity retention of only 63% after 50 cycles, and a low discharge voltage of ≈0.4 V.[49]

Although lignin-based biopolymers offer promising renewable, wood-derived alternatives to synthetic polymers, research on lignin-based RFBs remains in its early stages. Significant advancements in key performance metrics, such as specific gravimetric/volumetric capacity, energy density, kinetics and cycling stability, are still necessary to fully realize their potential.

In this study, we report, for the first time, the use of a low-cost sodium lignosulfonate (NaLS) aqueous catholyte for Zn-hybrid RFBs using quasi-neutral electrolytes. The inherent poor and sluggish electrochemical behavior observed for NaLS was effectively addressed by using carbon felts impregnated with carbons particles and employing an initial activation step that consists of an "in situ" electrochemical oxidation of lignin adducts within the electrochemical reactor. A RFB utilizing 10 mM NaLS catholyte and a Zn anode achieved an average cell voltage of 1.01 V and a volumetric capacity of 1.41 Ah L^{-1}. To further increase the capacity, the NaLS concentration was increased to 30 mM, which yielded a capacity of 3.52 Ah L^{-1}. Notably, the electrolyte exhibited an exceptionally low cost of 26 € kWh^{-1}.

2. Results and Discussion

2.1. Principle of Operation

Figure 1 illustrates the architecture and operating principle of the Zn/Lignosulfonate RFB, which employs a filter-press reactor design incorporating a cellulose dialysis membrane as the ionic separator. The positive electrode consists of an impregnated carbon felt, supported by an expanded graphite current collector, while the negative electrode is a zinc foil that also serves as the current collector. The anolyte is composed of an aqueous ZnSO$_4$ solution, and the posolyte is prepared by dissolving NaLS at various concentrations into the same ZnSO$_4$ solution to ensure electrolyte compatibility. During the charging process, Zn^{2+} ions in the anolyte are electrodeposited as metallic zinc on the negative electrode, while in the posolyte, quinonyl groups of

the LSs are oxidized to hydroxy-substituted species. The reverse reactions occur during discharge, with zinc metal dissolving back into Zn^{2+} and hydroxy groups being reduced back to quinonyl species, thereby completing the redox cycle.

### 2.2. Optimization of Carbon Felts Electrodes

Prior to the assembly of the RFB, we evaluate how the activation method of the felts and their composition influences the electrochemical behavior of lignin active species in the posolyte. This was investigated by cyclic voltammetry (CV) of a representative LS, that is 2.5 kDa NaLS, in 1 M ZnSO$_4$ aqueous electrolyte. The study began by optimizing the felt activation method and selecting appropriate carbon inks for impregnation (see **Table 1**). Two activation approaches—acid-activated felt (AAF) and thermally activated felt (TAF), were compared. Both showed similar CV profiles, each with a distinct oxidation peak around 0.2 V versus Ag/AgCl and a reduction peak near 0.1 V versus Ag/AgCl (**Figure 2** a,b). AAF also exhibited a secondary, less pronounced oxidation peak around 0.45 V versus Ag/AgCl. Hydrophilicity and electrical conductivity of TAF and AAF were also investigated. Both activation methods yielded hydrophilic felts capable of rapid ink absorption (see Supporting Information Video). Electrochemical impedance spectroscopy (EIS) revealed that TAF exhibited lower resistance (0.19 Ω cm^2) than AAF (0.27 Ω cm^2). The impregnation of the felts with carbon (90 wt% Ketjen Black (KB), ≈2.5 mg cm^{-2}) resulted in significant changes in the CV curves. Regardless of the activation method, two sets of reversible redox peaks emerged,

Table 1. Composition of carbon inks (% by wt).

Ink sample	KB [%]	AC [%]	PVDF [%]	CMC [%]
1	90	–	10	–
2	96	–	4	–
3	96	–	–	4
4	80	16	–	4
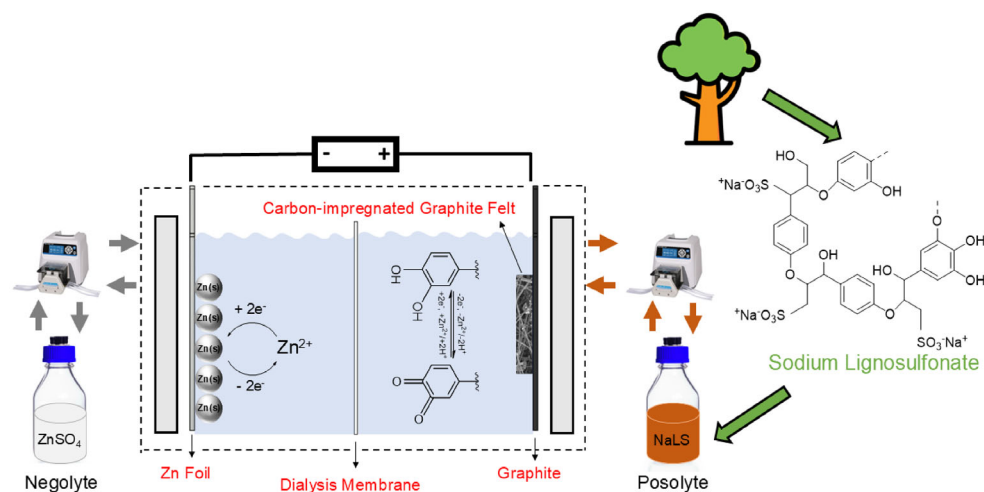
Figure 1. Schematic representation of Zn/NaLS hybrid RFB, illustrating the two half-reactions occurring in the lignin-based posolyte and at the Zn anode.
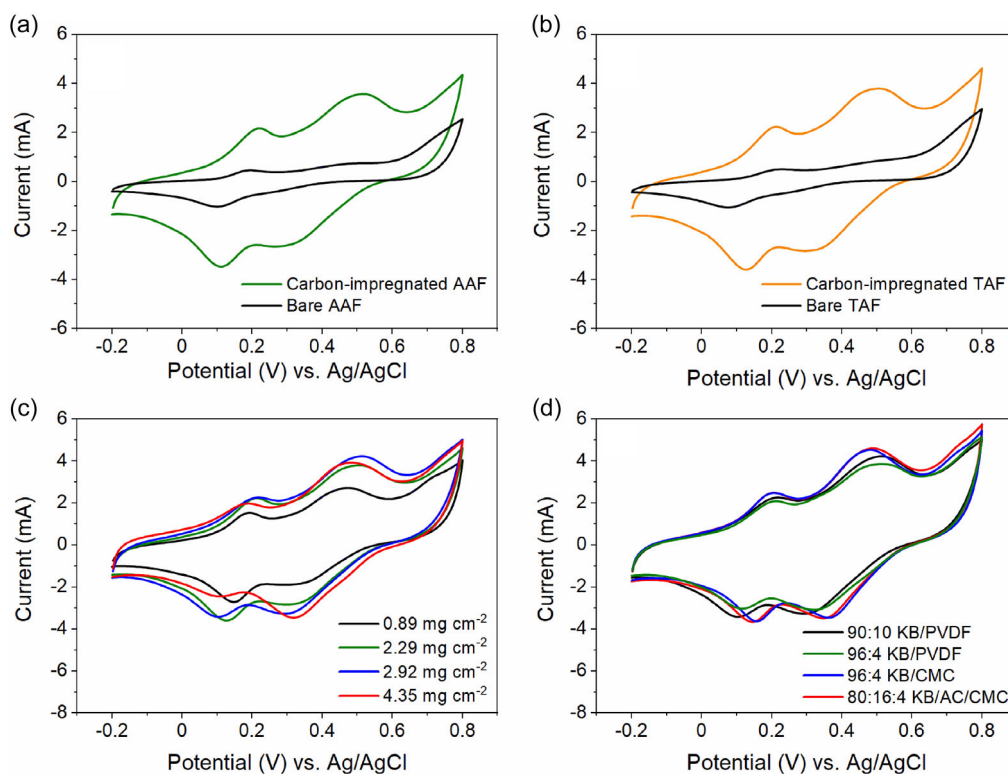
Figure 2. CV curves of 10 mM NaLS (2.5 kDa) in 1 M ZnSO$_4$, a) comparing nonimpregnated and carbon-impregnated carbon felts for AAF and b) TAF carbon felts (ink sample 1 in Table 1, mass loading of ≈2.5 mg cm^{-2}). c) Carbon-impregnated felts (KB and PVDF, 90:10 wt%) at different mass loading and d) impregnated felts with various carbon ink formulations (see Table 1), mass loading of ≈2.5 mg cm^{-2}.

with redox potentials ($E_{1/2}$) centered at ≈0.16 and 0.4 V, independent of the felt activation method (Figure 2 a,b). The peaks indicate the presence of two distinct redox processes, attributed to different functional groups within the NaLS.[50,51] This emphasizes the importance of carbon impregnation, as KB substantially enhances the surface area and the number of reaction sites, thereby mitigating the inherently quasireversible kinetics of LSs in low proton environments.[40] Between the two activation methods, TAF was selected for further studies due to its slightly higher peak intensities and narrower peak separation, likely due to its slightly lower electrical resistance, compared to AAF. Additionally, TAF offers practical advantages: It provides a more reproducible approach, eliminates the need for acidic solutions, and relies solely on thermal treatment—making it a simpler and more environmentally friendly option.

To optimize carbon loading in the impregnated felts, different KB mass loadings (ranging from 0.89 to 4.35 mg cm^{-2}) were evaluated. As shown in Figure 2c, the peak currents in the CVs increased at higher carbon loading, indicating an enhanced ease of the NaLS redox reactions on the electrode surface. Interestingly, the highest peak current was observed at a KB loading of 2.92 mg cm^{-2}, lower than the highest loading used in the study. This suggests that excessively high loadings may hinder NaLS mass transport within the electrode. A similar trend was reported for the VO^{2+}/VO$_2^+$ redox couple on mesoporous graphene-coated felts.[52] Based on these findings, an optimal mass loading in the range of 2–3 mg cm^{-2} was chosen.

The influence of binder type on NaLS electrochemistry was also evaluated by comparing polyvinylidene fluoride (PVDF) and carboxymethyl cellulose (CMC)-based carbon coatings. As shown in Figure 2d, the CVs obtained using CMC-based inks exhibited significantly higher peak currents and better redox kinetics than those with PVDF, underscoring the superior electrochemical performance in felts impregnated with carbon inks containing CMC binder. Furthermore, when the carbon content was increased from 90 to 96 wt% in the ink with PVDF, the performance declined. Consequently, CMC was selected as the preferred binder due to its water-processability, lower cost, and enhanced electrochemical behavior of NaLS-based electrolytes.[53] To improve processability without compromising performance, KB was partially substituted with activated carbon (AC), maintaining a total carbon content of 96 wt% and 4 wt% CMC. The resulting CVs showed minimal variation, indicating that AC substitution did not significantly affect the electrochemical response of NaLS. Additionally, the stability and the lifetime of the binders were evaluated using coin cells. The cells were galvanostatically cycled for 100 cycles at 0.25 A g^{-1} within two voltage windows: 0.2–1.6 V (representing the RFB operating voltage range) and 0.2–2 V (extending the upper voltage limit of the carbon felt). Both cells remained stable within the lower range, while noticeable degradation of the impregnated carbon felts occurred when extended to 2 V with both binders (Figure S1, Supporting Information). Since our RFB system operates within the stable window, either binder is technically suitable; however, CMC

Batteries & Supercaps

Research Article
doi.org/10.1002/batt.202500529

Chemistry Europe
European Chemical
Societies Publishing

was ultimately selected due to its lower cost and water-based formulation, making it a more sustainable and practical choice.

In summary, the various modifications applied to the impregnated felts—including binder type (PVDF vs. CMC), carbon:binder ratio (90:10 vs. 96:4), and the nature of carbons additives (KB vs. KB/AC), all resulted in a significant enhancement in the electrochemical response of lignin species compared to nonimpregnated electrodes. However, the differences among these impregnated felts themselves remained relatively minor, and their overall impact on the electrochemical behavior of NaLS was negligible. Notably, the inclusion of AC improved the mechanical handling and fabrication of the electrodes due to its higher surface area and better processability.[54,55] Based on these findings, a composition of 80:16:4 wt% of KB:AC:CMC was selected for further studies.

2.3. Electrochemical Activation of Lignin-Based Posolyte

It is important to note that all the cyclic voltammograms used in the optimization studies of the felt were recorded from the second scan onward. Interestingly, the first scan, conducted with a higher positive cutoff potential (1.1 V vs. 0.8 V), exhibited distinct behavior. As shown **Figure 3**a, a sharp increase in current is observed around 0.3 V, corresponding to an irreversible electrochemical oxidation process in the first cycle. This behavior is characteristic of an initial electrochemical activation process, during which the lignin structure undergoes oxidative modification, as reported elsewhere.[56] Specifically, hydroxyl (-OH) and methoxy (-OCH$_3$) groups on the aromatic ring are converted into redox-active o-quinone species—functionalities that are known to exhibit electrochemical reversibility in lignin and LSs.[40,41,57] This redox reversibility is a key functional attribute, directly linked to the chemical transformation of lignin's native functional groups during electrochemical activation in the first anodic scan. Specifically, the irreversible oxidation of phenolic and methoxy groups (demethoxylation) into o-quinones not only introduces additional redox-active sites but also improves the reversibility of the charge transfer processes within the electrode–electrolyte interface.

In subsequent scans, this oxidative transformation is reflected in the emergence of two well-defined and reversible redox peak pairs, centered at 0.42 and 0.17 V in Figure 3a, confirming the formation of stable redox-active sites. These findings highlight the critical role of in situ chemical modification of lignin in unlocking its electrochemical potential. The electro-oxidation of NaLS acts as a built-in "activation mechanism", enhancing the concentration of electrochemically addressable sites without requiring additional chemical synthesis or costly postprocessing. The synergistic combination of increased redox site density in the catholyte and an optimized electrode interface in carbon-impregnated felts led to enhanced charge storage capacity, which remained stable over cycling (as evidenced by the overlapping CV curves from cycles 2–5 in Figure 3a). As will be discussed later, the formation of these reversible quinone moieties during the first oxidation scan is essential for successful galvanostatic charge–discharge (GCD) cycling, necessitating an initial, extended charging step to fully activate the material via electrochemical oxidation.

2.4. Effect of Molecular Weight of Lignosulfonate (NaLS) on the Electrochemistry

While the previous optimization of carbon felt electrodes was conducted with 2.5 kDa NaLS, the electrochemical performance of a higher molecular weight variant (20 kDa) was also assessed using CV. The CV of 20 kDa NaLS exhibited a single, yet broad, pair of oxidation and reduction peaks, with $E_{1/2}$ centered at 0.45 V. This contrasts with the two well-defined redox peak pairs observed for the 2.5 kDa NaLS (Figure 3b). The difference in electrochemical profiles is likely attributed to the more complex and bulky structural backbone of the 20 kDa NaLS, which may influence electron transfer kinetics and redox site accessibility.[58] The 20 kDa NaLS demonstrated a slightly higher faradaic specific capacitance (343 C g^{-1}) compared to the 2.5 kDa NaLS (277 C g^{-1}), indicating that the higher molecular weight NaLS possesses slightly greater density of electrochemically active sites and, consequently, enhanced overall charge storage capability.
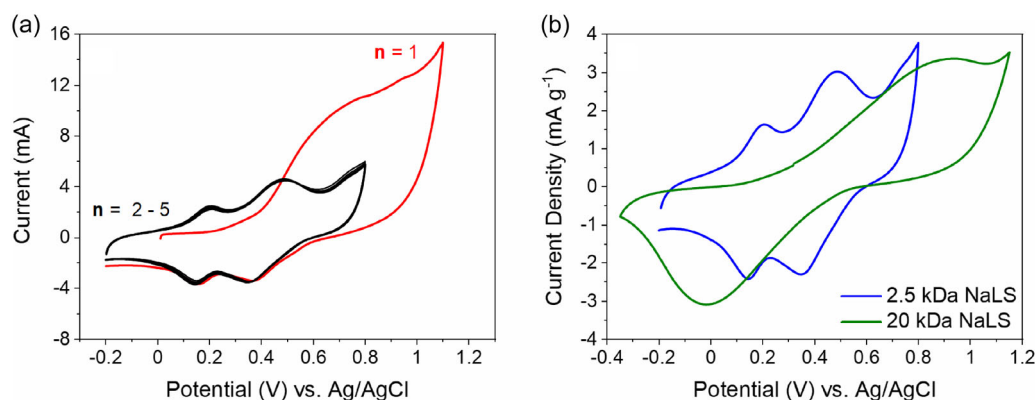
Figure 3. Cyclic voltammograms of a) 2.5 kDa NaLS, first five consecutives cycles and b) 2.5 and 20 kDa NaLS (second cycle) in 1 M ZnSO4 on a TAF impregnated with 80:16:4 KB/AC/CMC at 2.5 mV s^{-1}.

Batteries & Supercaps

Research Article
doi.org/10.1002/batt.202500529

Chemistry Europe
European Chemical
Societies Publishing

## 2.5. Electrochemical Performance of Zn/Lignosulfonate RFB

2.5.1. Effect of the Lignosulfonate Molecular Weight

The electrochemical performance of the Zn/Lignosulfonate RFB was evaluated using GCD tests at various C-rates, employing different posolyte compositions. The positive electrodes were based on the optimized impregnated felts prepared with a carbon mixture composed of 80:16:4 wt% KB:AC:CMC. Prior to the rate capability experiments, a preactivation step was performed by charging the battery up to 1.8 V at current densities of 2.5 and 5 mA cm^{-2}, using both 2.5 and 20 kDa NaLS posolytes (see Figure S2, Supporting Information). This step was necessary to generate redox-active o-quinone moieties through oxidative demethoxylation of the LS macromolecules.[42,59] Following this activation, both posolytes retained 20–30% of their initial charge capacity, indicating that a portion of the lignin moieties underwent irreversible oxidation during this first charge step. Future work will focus on optimizing the activation protocol to tailor the density and distribution of quinone functionalities.

Figure 4 and Figure S3 (Supporting Information) compares the electrochemical performance of Zn/NaLS RFBs, employing NaLS of different molecular weights (2.5 and 20 kDa). Figure 4a,b present the capacity–voltage profiles at a current density of 2.5 mA cm^{-2} while Figure S3 (Supporting Information) extend this analysis by showing the capacity–voltage profiles

at different current densities. The corresponding values of discharge capacities and CEs are depicted in Figure 4c,d, respectively. As shown in Figure 4b, the RFB employing the 20 kDa NaLS posolyte achieved the highest gravimetric discharge capacity of 9.74 mAh g^{-1} at 2.5 mA cm^{-2}, along with a CE of 83%. Further reductions in current density did not improve capacity and instead resulted in lower CEs. In contrast, the RFB using 2.5 kDa NaLS posolyte delivered a significantly lower capacity of 5.89 mAh g^{-1} at the same current density (Figure 4a). Although this capacity improved at lower current densities—reaching 8.1 mAh g^{-1} at 1.5 mA cm^{-2} while maintaining CEs above 90%—the gravimetric capacity remained notably lower than that of the 20 kDa NaLS across all tested conditions (Figure 4c).

This behavior aligns with its function as an anionic polyelectrolyte, however a direct comparison of the CV and the GCD can be misleading.[60,61] It's important to note that the CV (Figure 3b) is normalized based on the mass of active material in the catholyte, while the GCD (Figure 4a,b) is normalized by the electrode area. A more accurate comparison would involve assessing the CV results alongside GCD data at similar specific current densities—15 mA cm^{-2} for the 20 kDa NaLS and 2.5 mA cm^{-2} for the 2.5 kDa NaLS (from the areal currents in CV). When this comparison is made, the higher overall resistance observed in the CV for the 20 kDa sample is also evident in the corresponding GCD measurements. A notable advantage of the 20 kDa NaLS posolyte is its higher average discharge voltage—1.01 V versus 0.89 V for the
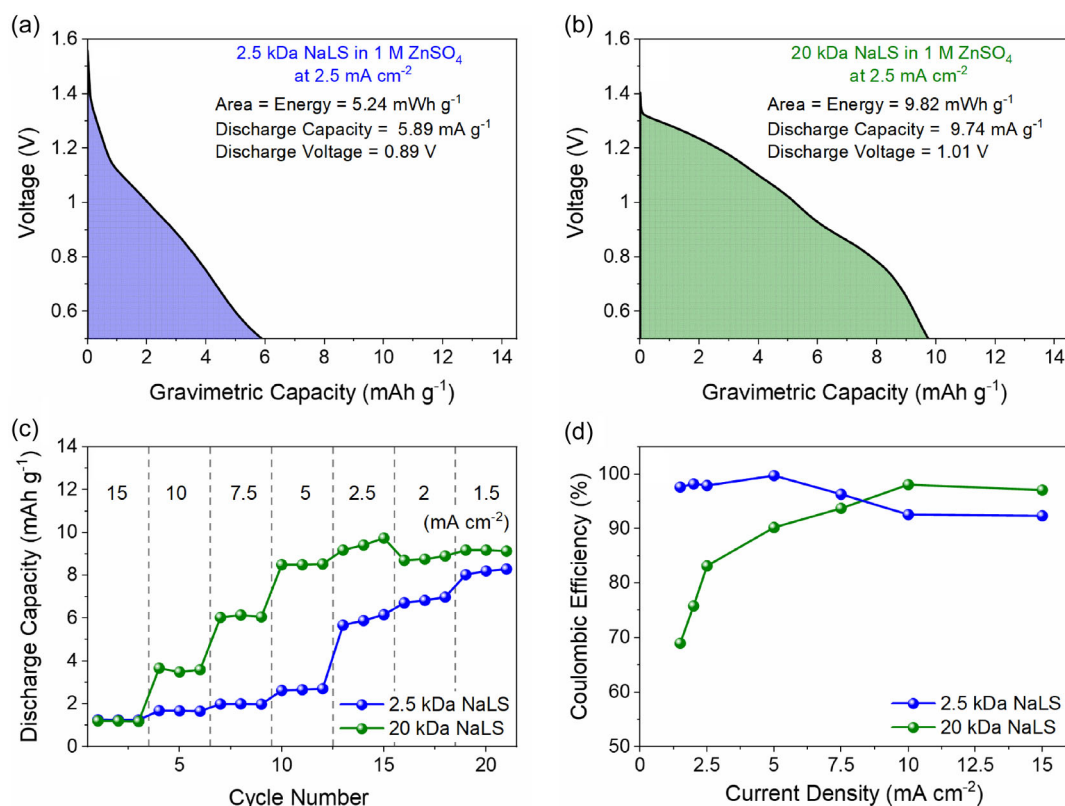
Figure 4. Specific capacity–voltage profiles of a) 10 mM 2.5 kDa NaLS and b) 10 mM 20 kDa NaLS 2.5 mA cm^{-2} to determine the average discharge voltage. Rate performance studies of Zn/NaLS RFBs in 1 M ZnSO$_4$ aqueous electrolytes for 10 mM 2.5 kDa NaLS and 10 mM 20 kDa NaLS. c) Gravimetric discharge capacity versus cycle number at different current density. d) Average CE during the rate capability test.

2.5 kDa NaLS—representing a 120 mV increase (Figure 4a,b). The combined benefits of higher discharge voltage and capacity for 20 kDa NaLS yield a remarkable higher specific energy of 9.82 Wh $kg^{-1}_{posolyte}$ versus 5.24 Wh $kg^{-1}_{posolyte}$ for 2.5 kDa NaLS. Considering these results, 20 kDa NaLS was selected as the posolyte active-material for further investigation.

2.5.2. Redox Mechanism of NaLS

The changes in the structure of NaLS in charged and discharged states was analyzed with Fourier transform infrared spectroscopy (FTIR) (Figure S4, Supporting Information). The pristine lignosulfonate (NaLS) exhibited a broad peak around 3400 cm^{-1}, attributed to aromatic –OH groups, and a peak at 2930 cm^{-1}, corresponding to C–H stretching in –OCH$_3$ groups.[62] Multiple peaks in the 1000–1130 cm^{-1} region was associated with C–O–C ether linkages.[63] Additionally, peaks at 1424, 1351, and 1328 cm^{-1} were assigned to –OH bending vibrations of the aromatic ring.[64]

As discussed before, electrochemical activation of NaLS (charging up to 1.8 V) induced structural changes. This is evidenced by the transformation of the 1100–1300 cm^{-1} region into a single, sharp, and intense peak, which corresponds to the vibration bands of guaiacyl units in NaLS.[65] Furthermore, the –OH band (a broad peak around 3400 cm^{-1}) became broader and shifted to a lower wavenumber, indicating structural reorientation and intermolecular interactions.

Importantly, the C–H stretching peak at 2930 cm^{-1} disappeared after activation, while a new small peak emerges around 1735 cm^{-1}, attributed to C=O stretching, suggesting the oxidation of methoxy groups to carbonyl functionalities. This carbonyl peak significantly decreases during discharge and reappears upon recharging to 1.6 V, indicating a reversible quinone–hydroquinone redox mechanism, which is typical of lignin-based redox-active materials.[66]
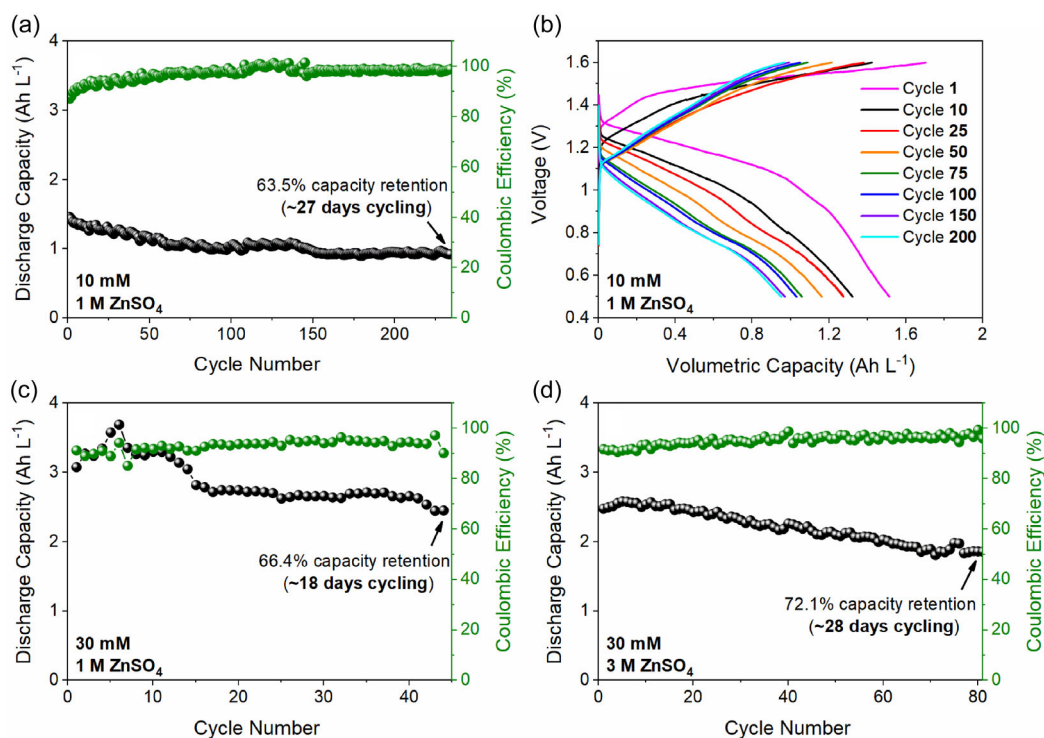
2.5.3. Optimization of the Lignin-Based Posolyte

To maximize the volumetric capacity of the Zn/NaLS RFB, the concentration of NaLS (20 kDa) in the posolyte was gradually increased from 10 to 30 mM. Further increase in concentration was avoided due to viscosity constraints, which could hinder the mass transport of the NaLS species. As shown in **Figure 5**a, this approach significantly boosted the volumetric capacity, increasing from 1.5 Ah L^{-1} with 10 mM NaLS to 3.52 Ah L^{-1} with 30 mM NaLS. However, this increase was not linear, as depicted in Figure 5b. This nonlinearity arises from a slight decline in gravimetric capacity with increasing NaLS concentration, which decreased from 9.74 to 5.94 mAh g^{-1} over this concentration range (Figure 5b). This reduced capacity utilization can be attributed to transport limitations in more concentrated solutions, where increased viscosity can hinder ion mobility and reduce overall charge transfer efficiency. Despite this, the overall gain in volumetric capacity remains highly favorable, demonstrating that the RFB can achieve substantial volumetric capacity improvements at higher NaLS concentrations. In fact, a quadratic fit of the data predicts a maximum discharge capacity of 3.53 Ah L^{-1} at 32.2 mM of NaLS, while a capacity of 3.52 Ah L^{-1} was already achieved at 30 mM. This indicates that the RFB is already operating near its maximum achievable discharge capacity under the current design and conditions.

The cyclability test of the battery was initially carried out using a posolyte concentration of 10 mM NaLS in 1 M ZnSO$_4$ (**Figure 6**a,b). The cell demonstrated stable cycling performance at 2.5 mA cm^{-2}, operating for 234 cycles ($\approx$27 days). After this extended period, the RFB retained 63.5% of its initial capacity. Notably, by the end of the experiment, only about 5 mL of negolyte remained in the reservoir. We observed that water migration from the negolyte reservoir to the posolyte reservoir occurred primarily during the activation cycle and continued gradually throughout the cycling process. This volume loss was attributed to the hydrogen evolution reaction (HER) and osmotic drag, driven by differences in ionic strength and viscosity between the posolyte and the negolyte, as well as osmotic pressure gradients.[67,68] This effect becomes even more pronounced at higher NaLS concentrations. Therefore, to mitigate the effects of electro-osmotic drag, the volume of the negolyte was doubled relative to that of the posolyte in further experiments where the concentration of NaLS was increased. As shown in Figure 6c, the Zn/NaLS RFB with a 30 mM posolyte (1 M ZnSO$_4$) retained 66% of its initial
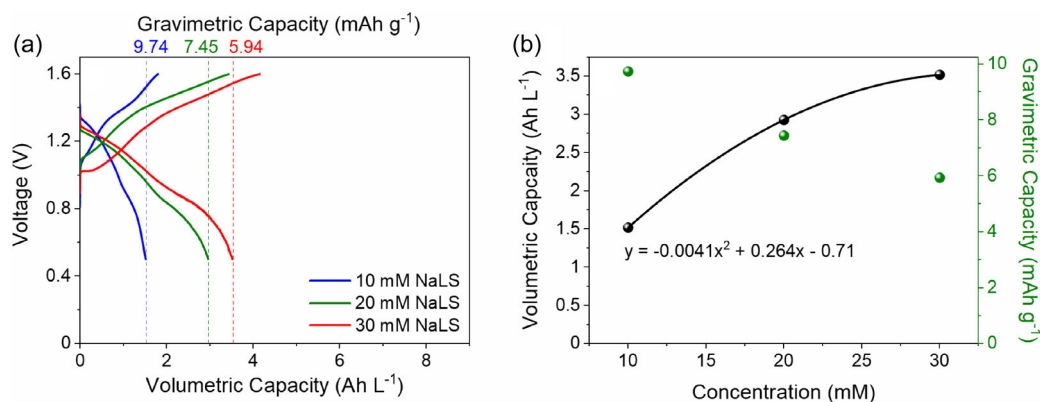
Figure 5. a) Voltage versus capacity profiles of Zn/NaLS RFBs in 1 M ZnSO$_4$ aqueous electrolyte at different NaLS concentrations—10, 20, and 30 mM, cycled at 2.5 mA cm^{-2}. b) Concentration of posolyte (mM) versus volumetric discharge capacity (Ah L^{-1}).

Batteries & Supercaps

Research Article
doi.org/10.1002/batt.202500529

Chemistry Europe
European Chemical
Societies Publishing

Figure 6. a) Cycling performance of Zn/NaLS (10 mM, 1 M ZnSO₄) RFBs cycled at 2.5 mA cm⁻² and b) representative charge–discharge cycles during long-term cyclability test. Cycling performance of Zn/NaLS (30 mM) RFBs cycled at 2.5 mA cm⁻² in c) 1 M ZnSO₄ and d) 3 M ZnSO₄ aqueous electrolytes.

capacity after 44 cycles at 2.5 mA cm⁻², compared to 81% retention, for the battery using 10 mM NaLS posolyte (Figure 6a and Table S1, Supporting Information). The lower capacity retention observed with 30 mM NaLS can be further explained by the occurrence of parasitic reactions at the Zn anode. As the posolyte concentration increases, the cell undergoes more demanding charge/discharge cycles due to the higher accessible capacity, placing greater stress on the Zn electrode. This enhances the likelihood of side reactions, contributing to accelerated capacity fade.

Enhanced stability in 3 M ZnSO₄ arises primarily from improved Zn plating/stripping and suppressed parasitic hydrogen evolution at the Zn electrode.[69,70] In more dilute electrolytes (e.g., 1 M), the higher water activity and lower ionic strength favor HER during charging, which competes with $Zn^{2+} \rightarrow Zn$ (plating, cathodic), lowers CE, promotes porous/dendritic deposits, and accelerates instability. By contrast, at higher concentration the reduced water activity and altered Zn^{2+} solvation/double-layer structure (including sulfate adsorption) disfavor HER and promote denser, more uniform Zn deposits, yielding higher CE and more stable cycling. This mechanistic picture is consistent with prior ZnSO₄ studies.[71,72] We note that excessively concentrated electrolytes can increase viscosity and mass-transport losses; 3 M provides a practical balance between HER suppression and acceptable transport in our cells.

Hence, to achieve a balance between high capacity and stability, we also prepared electrolytes using higher concentration of ZnSO₄ as supporting salt and we investigated the effect of posolyte composition (NaLS and ZnSO₄ concentration) on the

posolyte resistance by EIS (Figure S5, Supporting Information). We found that as the NaLS concentration in the electrolyte increased, the ohmic resistance also increased, specifically at 1 M ZnSO₄ denoting the insulating nature of NaLS. Moreover, resistance of the system at 3 M ZnSO₄ is lower than at 1 M ZnSO₄ at higher concentrations of NaLS (20 and 30 mM), which might be beneficial for the overall battery performance.

Therefore, to address the stability limitations observed with 1 M ZnSO₄ supporting salt, we assembled and tested a RFB using 30 mM NaLS in 3 M ZnSO₄ as posolyte and 3 M ZnSO₄ as negolyte. The cycling performance of such RFBs was assessed through GCD cycling at 2.5 mA cm⁻² (Figure 6d and Figure S6b, Supporting Information) and compared with the battery using 30 mM NaLS in 1 M ZnSO₄ (Figure 6c and Figure S6a, Supporting Information). The RFB with 30 mM NaLS in 1 M ZnSO₄ achieved a higher maximum discharge capacity of 3.69 Ah L⁻¹, compared to 2.58 Ah L⁻¹ for the RFB with 3 M ZnSO₄. This lower capacity at higher ZnSO₄ concentration might be attributed to increase viscosity-induced polarization of the RFB as the ZnSO₄ concentration increased.[73] Nevertheless, as shown in Figure 6d, the higher salt concentration significantly improved cycling stability, primary by substantially enhancing the efficiency of Zn plating/stripping reaction in the anode.[69] The RFB with a 3 M ZnSO₄ retained 72% of its capacity after 80 cycles, whereas the one with 1 M ZnSO₄ retained only 66% before experiencing a shorting failure after 44 cycles. Additionally, the cell with 3 M ZnSO₄ exhibited a longer stable cycling duration of 28 days, compared to 18 days for the 1 M ZnSO₄ cell. It is worth noting that the average CE was slightly higher in the 3 M ZnSO₄ electrolyte, exceeding 95%,

Batteries & Supercaps

Research Article
doi.org/10.1002/batt.202500529

**Chemistry
Europe**
European Chemical
Societies Publishing

compared to ≈93% in the 1 M ZnSO$_4$ electrolyte. It is also important to note that, increased zinc utilization in both RFBs with 30 mM NaLS—regardless of whether 1 M or 3 M ZnSO$_4$ was used—led to significant anode corrosion, a phenomenon not observed in the RFB using 10 mM NaLS posolyte. Digital photographs of the Zn anodes postcycling (Figure S7, Supporting Information) reveal severe corrosion and anode degradation in both cases using the 30 mM posolyte, with particularly extensive damage observed in the 1 M ZnSO$_4$ system, further emphasizing the critical impact of electrolyte concentration on anode stability.

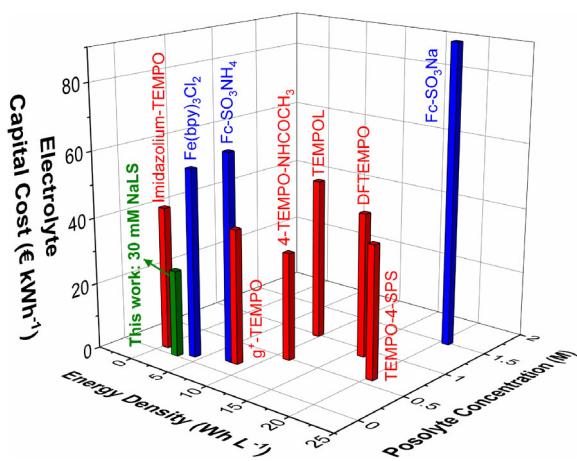## 2.6. Assessment of Electrolyte Capital Cost and Comparison with the State-of-Art

One of the key motivations for designing an aqueous RFB using this nonsynthetic, natural lignin-based material as a posolyte was to leverage its low raw material cost (0.3 $ kg^{-1}).[74] Given the promising performance of the Zn/NaLS RFB, an elementary cost analysis of the electrolyte was conducted (details provided in the Supporting Information). For a more meaningful comparison, this analysis was extended to include the most representative hybrid Zn/Organic RFB chemistries reported in the

literature, mainly using TEMPO and Fe-based derivatives as posolytes (refer to Supporting Information and Table S2—S5 for details).

Figure 7 and Table S5 (Supporting Information) present a comparative assessment of the most representative state-of-the-art aqueous Zn/Organic RFB chemistries. In addition to the calculated electrolyte capital cost, this analysis also considers critical performance parameters, including discharge voltage, electrolyte concentration, energy density, and membrane type, to provide a comprehensive overview. The ZnSO$_4$/NaLS system presented in this work exhibits a moderate average discharge voltage of 1 V, which is comparable to several reported Zn/organic RFBs such as ZnBr$_2$/Fc-SO$_3$Na (0.9 V) and ZnCl$_2$/4-TEMPO-NHCOCH$_3$ (1.45 V). Although the NaLS concentration (30 mM) is lower than in most other systems, this is offset by its ability to deliver a reasonable energy density of 2.58 Wh L^{-1}. Notably, this work employed a cellulose dialysis membrane, whereas all other studies utilized either commercial ion-exchange membranes or custom-synthesized alternatives.

Regarding the posolyte capital cost, the Zn/NaLS RFB exhibited the lowest electrolyte capital cost at 26 € kWh^{-1}, primary due to the significantly lower raw material cost ofL Ss. Furthermore, as a macromolecule, LS is compatible with cost-effective SEM, unlike most aqueous Zn/Organic RFBs that require more expensive membranes. This combination of low raw material cost and reduced membrane expense positions the Zn/NaLS RFB as a highly competitive option for cost-effective energy storage.

Although the energy density achieved in this study is moderate when compared to Zn-hybrid systems using synthetic small organic molecules, the Zn/NaLS RFB demonstrates a substantial improvement over previously reported lignin-based RFBs. **Table 2** presents a comparative overview of the performance of the RFB developed in this work against previously reported polymer and lignin-based Zn-hybrid RFBs. The Zn/NaLS hybrid RFB developed in this work demonstrates significant performance improvements over previously reported—the Zn/10 mM NaLS RFB achieved an average discharge voltage of 1.01 V and an initial capacity of 1.41 Ah L^{-1}, notably outperforming other lignin-based RFBs such as LSs (0.325 Ah L^{-1}) and soda lignin (0.19 Ah L^{-1}). The system also exhibits excellent cycling stability, maintaining a low-capacity fade rate of 0.15% per cycle over 234 cycles, comparable to or better than

Figure 7. Comparison of electrolyte capital cost and energy density of reported aqueous Zn/organic hybrid RFB posolytes (Imidazolium-TEMPO,[76] g$^+$-TEMPO,[77] 4-TEMPO-NHCOCH$_3$,[78] TEMPOL,[79] DFTEMPO,[80]TEMPO-4-SPS[81], Fe(bpy)$_3$Cl$_2$,[82] Fc-SO$_3$NH$_4$,[83]and Fc-SO$_3$Na[84]) with the electrolyte used in this study (30 mM NaLS with 3 M ZnSO$_4$ as supporting salt).

Table 2. Comparison of various polymer and lignin-based Zn-hybrid RFBs.

Aqueous negolyte	Aqueous posolyte	Electrolyte type/ Membrane	Concentration of lignin [M]	Capacity [Ah L^{-1}]	Discharge voltage [V]	Cycles/Capacity fade [% cycle^{-1}]	References
Br$_2$/HBr	Lignosulfonate	Acidic/Nafion 212	0.1	0.325	<0.35	–	[45]
pBQ	MHQ	Acidic/Nafion 211	0.001	0.112	<0.2	250/0.05	[46]
Mixed G-S	K$_4$[Fe(CN)$_6$]	Alkaline/Nafion 117	0.01	0.104	<0.5	200/0.11	[47]
Mixed LAQDs	K$_4$[Fe(CN)$_6$]	Alkaline/Nafion	0.01	0.144	<0.5	200/0.095	[48]
Soda lignin	K$_4$[Fe(CN)$_6$]	Alkaline/Nafion 212	0.0035	0.19	≈0.4	50/0.73	[49]
ZnSO$_4$	NaLS	Quasineutral/Cellulose	0.01/0.03	1.41/2.58	1.01/0.93	234/0.1580/0.35	This work

most systems reported. Increasing the NaLS concentration to 30 mM further enhanced the volumetric capacity to 2.58 Ah L^{-1} with 3 M ZnSO$_4$ as the supporting electrolyte. These enhancements are attributed to a combination of in situ electrochemical activation of quinone functionalities in the LSs backbone and the use of carbon-impregnated felts, which improve electrode kinetics and redox site accessibility. This strategy maximizes catholyte utilization and enhances reversibility, mitigating the limitations traditionally associated with lignin-based systems.

3. Conclusion

In summary, a cost-effective Zn/Organic hybrid RFB utilizing commercially available NaLS as an aqueous posolyte active material has been successfully demonstrated. The NaLS redox-active compound showed significantly improved electrochemical behavior on carbon-impregnated felts with prominent and well-defined redox peaks. Notably, the NaLS with a higher molecular weight (20 kDa) exhibited a significantly higher gravimetric discharge capacity (9.74 mAh g^{-1}) compared to its lower molecular weight counterpart (2.5 kDa, 5.89 mAh g^{-1}), likely due to improved adsorption and more effective access to redox-active sites.

Although the energy density of the system remains modest compared to synthetic small-molecule-based Zn/RFBs, the electrochemical performance exceeds that of previously reported lignin-based RFBs, both in terms of capacity and voltage. These improvements stem from the synergistic effects of LSs activation and optimized electrode architecture which improve electrode kinetics and redox site accessibility. This strategy maximizes catholyte utilization and enhances reversibility, mitigating the limitations traditionally associated with lignin-based systems. Importantly, the use of naturally derived redox-active species and inexpensive cellulose membranes positions the system as a sustainable and scalable candidate for long-duration, grid-scale energy storage. Specifically, the low raw material cost of NaLS and the compatibility with cost-effective cellulose membrane offer significant economic benefits compared to other systems relying on more costly catholytes and membranes. This positions the Zn/NaLS RFB as a promising alternative for scalable energy storage, where cost reduction and sustainability issues are critical factors.

The moderate energy density, likely due to the partial redox participation of NaLS and their limited solubility, can be addressed through several optimization strategies. Potential approaches include the use of electrolyte additives, acid-compatible negolytes, optimization of in situ activation step, and the depolymerization of LS to enhance electrochemical activity, increase capacity, and improve overall RFB performance. To sum up, this proof-of-concept RFB demonstrates that NaLS derived from the pulp and paper industry presents a cost-effective, sustainable, and environmentally friendly alternative to synthetic polymers, supporting the development of economically viable, large-scale energy storage solutions.

4. Experimental Section

Materials and Chemicals

Two NaLS (2.5 and 20 kDa molecular weight) provided by Borregaard Lignotech, and zinc sulfate heptahydrate (ZnSO$_4$·7H$_2$O; Sigma–Aldrich, >99%) were used as received; dissolved in ultrapure Mili-Q water (H$_2$O) to prepare aqueous electrolytes. KB (EC-600 JD) and AC (NORIT DLC Supra 50) were used as received. Carbon felt (grade GFD 4.6 EA) and expanded graphite (1 mm thickness) were purchased from SGL Carbon GmbH. Zinc foil (thickness: 0.25 mm) was purchased from Thermo Fisher Scientific (99.98% metal basis) and polished with sandpaper prior to use. A cellulose-based dialysis membrane with an MWCO of 1000 g mol^{-1} and diameter of 45 mm (Spectra/Por 1) was provided by Carl Roth.

Impregnation of Carbon Felt Positive Electrodes

Prior to impregnation, the carbon felts were activated through one of two methods: thermal activation or acid activation. In the thermal activation process, the felts were heated at 400 °C for 4 h. For acid activation, the felts were treated for 5 h at 80 °C in an acidic solution consisting of a 3:1 volume ratio of sulfuric acid (H$_2$SO$_4$) and nitric acid (HNO$_3$). After activation, the felts were thoroughly washed with water until neutral pH was reached and dried under vacuum at 100 °C.

Four carbon ink formulations, detailed in Table 1, were used to impregnate the AC felts. Carbon inks were prepared using various weight ratios of KB, AC, and two binders: PVDF and CMC. For PVDF, a mixture of N-methyl pyrrolidone (NMP) and iso-propanol (IPA) was used as the dispersion medium, while for CMC-based inks, a solvent mixture of water and IPA was used. Initially, the carbon materials were dispersed in their respective solvent mixture and homogenized using tip sonication for 5 min, followed by 60 min of sonication in an ultrasonic bath. After homogenization, the respective binder solution as added to the carbon dispersion, and the mixture was stirred overnight at room temperature.

The impregnated carbon felts were prepared using a modified solution-coating method,[75] in which they were immersed in 20 mL of carbon ink, sonicated in an ultrasonic bath for 5 min, and dried overnight under vacuum at 80 °C. Impregnated carbon felts with varying mass loadings (up to 4.5 mg cm^{-2}) were prepared to evaluate their effect on the electrochemical properties of LS, focusing on improvements in surface area and conductivity.

Electrochemical Characterization of Lignin-Based Posolyte: Cyclic Voltammetry (CV)

CV tests were carried out in a three-electrode electrochemical cell containing 25 mL of the electrolyte. The catholyte consisted of NaLS: 10 mM of either 2.5 or 20 kDa molecular weight, dissolved in ZnSO$_4$ (1 M). An Ag/AgCl electrode (3 M NaCl) served as the reference electrode, a platinum mesh as the counter electrode, and a disc-shaped impregnated carbon felt (10 mm diameter) as the working electrode. All the CV measurements were conducted at a scan rate of 2.5 mV s^{-1}.

The capacitance from the CV curves was determined by integrating the I versus E plot for reduction (reverse scan). It was calculated using the formula,

$$Q = \int_{E1}^{E2} I(V)dV/sm \qquad (1)$$

Batteries & Supercaps

Research Article
doi.org/10.1002/batt.202500529

Chemistry Europe
European Chemical
Societies Publishing

where s is the scan rate in $V\,s^{-1}$, m is the mass (g) of NaLS, and E_1 and E_2 are the voltage limits in V.

Electrochemical Characterization of Lignin-bBased Posolyte: Electrochemical Impedance Spectroscopy (EIS)

The electrical conductivity of the activated felts was measured under compression using a coin cell configuration. The coin cell consisted of a 10 mm diameter (4.6 mm thick) activated felt electrode placed between two 16 mm Cu current collectors. The cell was secured in a four-point connection coin cell holder (CCH-1 from Biologic), and EIS was performed. The EIS measurement was conducted at a 0 V bias with a 10 mV amplitude ($V_{rms} \approx 7.07$ mV), spanning a frequency range from 200 to 2 kHz. The area-specific resistance (ρ_{el}) was calculated using the formula $\rho_{el}(\Omega cm^2) = RA$, where R represents the internal ohmic resistance of the cell and A is the contact area of the felt.

EIS measurements with varying NaLS and $ZnSO_4$ concentrations were conducted in a coin cell to examine the effect of the electrolyte conductivity on the ohmic resistance of the cell. The coin cells were assembled using two 16 mm 316 SS spacers separated by porous Whatman glass microfiber filters (Grade GF/D) with a diameter of 19 mm and an effective thickness of $117.05 \pm 0.52\ \mu m$, soaked with $\approx 300\ \mu L$ of LS and $ZnSO_4$ electrolyte. The EIS measurement of the coin cell was conducted at 0 V bias, with an amplitude of 10 mV ($V_{rms} \approx 7.07$ mV) over a frequency range of 500 to 1 kHz.

Performance Assessment of Zn/Lignosulfonate RFB: Reactor Assembly

Zn/Lignosulfonate RFB reactor were assembled using a filter-pressed reactor. The reactor consisted of a rectangular cellulose dialysis membrane (9.5 cm × 5 cm), expanded graphite as the positive current collector, a square impregnated carbon felt (3 cm × 3 cm) as the positive electrode substrate, and a Zn foil ($\approx 16\ cm^2$ geometric area) serving as both the negative electrode and current collector. Two Viton gaskets (each 1 mm thick) were used for sealing the posolyte side, while three were used on the negolyte side to ensure tight assembly. Prior to assembly, the dialysis membranes were soaked in H_2O for a minimum of 12 h to ensure proper hydration and flexibility. Electrolyte circulation was maintained using a MasterFlex L/S peristaltic pump, fitted with MasterFlex nonphthalate PVC tubing (inner diameter: 0.125 inches) and compatible pump heads. A constant flow rate of 15 mL min^{-1} was applied throughout the experiments.

NaLS electrolytes were prepared by dissolving 10, 20, or 30 mM, in either 1 or 3 M $ZnSO_4$ aqueous solution. It is important to note that these concentrations are based on the number-average molar mass provided by the supplier and does not directly reflect the amount of redox-active phenolic groups present in NaLS. 30 mL of these NaLS solutions were used as the posolyte. It was ensured that the negolyte was not capacity-limiting. The same concentration of Zn salt in the negolyte was used as the supporting electrolyte for the posolyte. Prior to the RFB experiments, the electrolytes were degassed with argon for 30 min, followed by continuous argon purging into the headspace of the electrolyte tanks throughout the measurements to prevent oxygen contamination.

Performance Assessment of Zn/Lignosulfonate RFB: Galvanostatic Charge-Discharge

To evaluate the electrochemical stability and lifetime of impregnated carbon felts with different binders GCD tests in a coin cell was performed. The coin cells were assembled using Zn foil as the anode, Whatman separators soaked in 1 M $ZnSO_4$ as the electrolyte, and thermally AC felts impregnated with carbon inks containing either CMC or PVDF as the cathode. The cells were galvanostatically within two voltage windows: 0.2–1.6 and 0.2–2 V.

The flow cells were galvanostatically charged and discharged between voltages cutoffs of 1.6 and 0.5 V, respectively. It is important to note that during the first cycle, the NaLSs were consistently electrochemically charged up to a higher upper voltage limit of 1.8 V to facilitate the "activation" of the lignin posolyte, as discussed earlier. Charge and discharge experiments were performed at different current densities normalized to the geometric area of the impregnated-carbon felt cathode substrate.

All the electrochemical tests were performed using a Biologic VMP 300 potentiostat.

Structural Characterization: Fourier Transform Infrared (FTIR) Spectroscopy

The FTIR spectroscopy in attenuated total reflectance (ATR) mode was employed to investigate the reaction mechanism of solid NaLS samples. A RFB was assembled as outlined in Section "Reactor Assembly", utilizing a catholyte composed of 10 mM NaLS (20 kDa) in 1 M $ZnSO_4$ and a 1 M $ZnSO_4$ anolyte. GCD cycling was performed, during which catholyte samples ($\approx 500\ \mu L$) were collected at selected cell voltages—1.8 and 1.6 V during the charging process, and 0.5 V during discharge. The collected samples were immediately quenched in liquid nitrogen, freeze-dried for 24 h, and subsequently vacuum-dried at 50 °C for 12 h to ensure complete removal of residual moisture. The resulting solid samples were then analyzed via FTIR spectroscopy.

Acknowledgements

Conflict of Interest

The authors declare no conflict of interest

Author Contributions

Athul Seshadri Ramanujam: writing—original draft, methodology, investigation, formal analysis, data curation, conceptualization. **Nagaraj Patil**: writing—review & editing, methodology, validation, supervision, funding acquisition. **Paula Navalpotro**: writing—review & editing, validation, supervision. **Rebeca Marcilla**: writing—review & editing, validation, supervision, resources, project administration, methodology, funding acquisition.

Batteries & Supercaps

Research Article
doi.org/10.1002/batt.202500529

**Chemistry
Europe**

European Chemical
Societies Publishing

Data Availability Statement

Data will be openly available in Zenodo once the article is accepted.

[1] X. Yuan, C.-W. Su, M. Umar, X. Shao, O.-R. Lobonţ, *J. Environ. Manage.* **2022**, *308*, 114648.

[2] Y. Liang, R. Kleijn, E. Van Der Voet, *Appl. Energy* **2023**, *346*, 121400.

[3] G. Notton, M.-L. Nivet, C. Voyant, C. Paoli, C. Darras, F. Motte, A. Fouilloy, *Renewable Sustainable Energy Rev.* **2018**, *87*, 96.

[4] J. A. Dowling, K. Z. Rinaldi, T. H. Ruggles, S. J. Davis, M. Yuan, F. Tong, N. S. Lewis, K. Caldeira, *Joule* **2020**, *4*, 1907.

[5] M. Skyllas-Kazacos, M. H. Chakrabarti, S. A. Hajimolana, F. S. Mjalli, M. Saleem, *J. Electrochem. Soc.* **2011**, *158*, R55.

[6] B. R. Chalamala, T. Soundappan, G. R. Fisher, M. R. Anstey, V. V. Viswanathan, M. L. Perry, *Proc. IEEE.* **2014**, *102*, 976.

[7] C. Lotspeich, in Proceedings of the 2002 EESAT Conference, San Francisco, CA, USA **2022**

[8] A. Trovò, M. Rugna, N. Poli, M. Guarnieri, *Ceram. Int.* **2023**, *49*, 24487.

[9] C. Doetsch, A. Pohlig, *Future Energy*, Elsevier, Amsterdam **2020**, pp. 263–277.

[10] A. Nasimifar, J. Mehrabani, *Int. J. Min. Geo Eng.* **2022**, *56*, 361.

[11] K. E. Rodby, M. L. Perry, F. R. Brushett, *J. Power Sources* **2021**, *506*, 230085.

[12] J. Noack, L. Wietschel, N. Roznyatovskaya, K. Pinkwart, J. Tübke, *Energies* **2016**, *9*, 627.

[13] T. Liu, X. Wei, Z. Nie, V. Sprenkle, W. Wang, *Adv. Energy Mater.* **2016**, *6*, 1501449.

[14] B. Hu, C. DeBruler, Z. Rhodes, T. L. Liu, *J. Am. Chem. Soc.* **2017**, *139*, 1207.

[15] Y. Liu, Q. Chen, P. Sun, Y. Li, Z. Yang, T. Xu, *Mater. Today Energy* **2021**, *20*, 100634.

[16] N. Goujon, N. Casado, N. Patil, R. Marcilla, D. Mecerreyes, *Prog. Polym. Sci.* **2021**, *122*, 101449.

[17] E. Y. Kozhunova, N. A. Gvozdik, M. V. Motyakin, O. V. Vyshivannaya, K. J. Stevenson, D. M. Itkis, A. V. Chertovich, *J. Phys. Chem. Lett.* **2020**, *11*, 1.

[18] Z. Li, T. Jiang, M. Ali, C. Wu, W. Chen, *Energy Storage Mater.* **2022**, *50*, 105.

[19] Y. Y. Lai, X. Li, Y. Zhu, *ACS Appl. Polym. Mater.* **2020**, *2*, 113.

[20] M. T. Tsehaye, G. Mourouga, T. J. Schmidt, J. O. Schumacher, S. Velizarov, B. Van Der Bruggen, F. Alloin, C. Iojoiu, *Renewable Sustainable Energy Rev.* **2023**, *173*, 113059.

[21] T. Janoschka, N. Martin, M. D. Hager, U. S. Schubert, *Angew. Chem., Int. Ed.* **2016**, *55*, 14427.

[22] K. Hatakeyama-Sato, T. Nagano, S. Noguchi, Y. Sugai, J. Du, H. Nishide, K. Oyaizu, *ACS Appl. Polym. Mater.* **2019**, *1*, 188.

[23] A. Kumar, B. P. Tripathi, *Electrochim. Acta* **2024**, *480*, 143906.

[24] T. Janoschka, N. Martin, U. Martin, C. Friebe, S. Morgenstern, H. Hiller, M. D. Hager, U. S. Schubert, *Nature* **2015**, *527*, 78.

[25] T. Hagemann, M. Strumpf, E. Schröter, C. Stolze, M. Grube, I. Nischang, M. D. Hager, U. S. Schubert, *Chem. Mater.* **2019**, *31*, 7987.

[26] W. Yan, C. Wang, J. Tian, G. Zhu, L. Ma, Y. Wang, R. Chen, Y. Hu, L. Wang, T. Chen, J. Ma, Z. Jin, *Nat. Commun.* **2019**, *10*, 2513.

[27] P. Rohland, E. Schröter, O. Nolte, G. R. Newkome, M. D. Hager, U. S. Schubert, *Prog. Polym. Sci.* **2022**, *125*, 101474.

[28] Z. Deller, L. A. Jones, S. Maniam, *Green Chem.* **2021**, *23*, 4955.

[29] G. L. Soloveichik, *Chem. Rev.* **2015**, *115*, 11533.

[30] J. Winsberg, T. Janoschka, S. Morgenstern, T. Hagemann, S. Muench, G. Hauffman, J. Gohy, M. D. Hager, U. S. Schubert, *Adv. Mater.* **2016**, *28*, 2238.

[31] T. Pham-Truong, Q. Wang, J. Ghilane, H. Randriamahazaka, *ChemSusChem* **2020**, *13*, 2142.

[32] R. K. Gautam, J. J. McGrath, X. Wang, J. J. Jiang, *J. Am. Chem. Soc.* **2024**, *146*, 28414.

[33] Y. Zhao, S. Si, C. Liao, *J. Power Sources* **2013**, *241*, 449.

[34] A. Fernández-Benito, F. J. Rivera-Gálvez, P. Cisneros-Ruiz, R. Sanz-Horta, C. F. Jasso-Gastinel, M. A. López-Manchado, J. Carretero-González, *Mater. Today Chem.* **2023**, *27*, 101271.

[35] I. A. Volodin, K. Wulf, F. Tzschoeckell, S. Stumpf, S. Hoeppener, N. Fritz, C. F. Morales-Reyes, T. Wichard, N. Ueberschaar, C. Stolze, M. D. Hager, U. S. Schubert, *J. Mater. Chem. A* **2024**, *12*, 4806.

[36] I. Haq, P. Mazumder, A. S. Kalamdhad, *Bioresour. Technol.* **2020**, *312*, 123636.

[37] C. Vasile, M. Baican, *Polymers* **2023**, *15*, 3177.

[38] H. Y. Jung, J. S. Lee, H. T. Han, J. Jung, K. Eom, J. T. Lee, *Polymers* **2022**, *14*, 673.

[39] L. Dessbesell, M. Paleologou, M. Leitch, R. Pulkki, C. Xu, *Renewable Sustainable Energy Rev.* **2020**, *123*, 109768.

[40] G. Milczarek, *Langmuir* **2009**, *25*, 10345.

[41] F. N. Ajjan, M. J. Jafari, T. Rębiś, T. Ederth, O. Inganäs, *J. Mater. Chem. A* **2015**, *3*, 12927.

[42] T. Rębiś, T. Y. Nilsson, O. Inganäs, *J. Mater. Chem. A* **2016**, *4*, 1931.

[43] T. Rębiś, G. Milczarek, *Electrochim. Acta* **2016**, *204*, 108.

[44] X. Yang, Y. Zhang, M. Ye, Y. Tang, Z. Wen, X. Liu, C. C. Li, *Green Chem.* **2023**, *25*, 4154.

[45] A. Mukhopadhyay, J. Hamel, R. Katahira, H. Zhu, *ACS Sustainable Chem. Eng.* **2018**, *6*, 5394.

[46] W. Schlemmer, P. Nothdurft, A. Petzold, G. Riess, P. Frühwirt, M. Schmallegger, G. Gescheidt-Demner, R. Fischer, S. A. Freunberger, W. Kern, S. Spirk, *Angew. Chem., Int. Ed.* **2020**, *59*, 22943.

[47] L. Jiao, M. Sun, J. Yang, W. Yang, H. Dai, *Ind. Crops Prod.* **2022**, *187*, 115431.

[48] L. Jiao, M. Sun, J. Yang, W. Yang, H. Dai, *Int. J. Biol. Macromol.* **2023**, *229*, 236.

[49] M. Chakraborty, M. B. Vives, O. Y. Abdelaziz, G. Henriksson, R. W. Lindström, C. P. Hulteberg, A. Khataee, *ACS Sustainable Chem. Eng.* **2024**, *12*, 15409.

[50] A. Chen, E. I. Rogers, R. G. Compton, *Electroanalysis* **2010**, *22*, 1037.

[51] S. Berling, S. Mavrikis, N. Patil, E. García - Quismondo, J. Palma, C. Ponce De León, *Electrochem. Commun.* **2022**, *142*, 107339.

[52] D. O. Opar, R. Nankya, J. Lee, H. Jung, *Electrochim. Acta* **2020**, *330*, 135276.

[53] S. F. Lux, F. Schappacher, A. Balducci, S. Passerini, M. Winter, *J. Electrochem. Soc.* **2010**, *157*, A320.

[54] Y. Holade, C. Morais, K. Servat, T. W. Napporn, K. B. Kokoh, *Phys. Chem. Chem. Phys.* **2014**, *16*, 25609.

[55] J. Pokrzywinski, J. K. Keum, R. E. Ruther, E. C. Self, M. Chi, H. M. Iii, K. C. Littrell, D. Aulakh, S. Marble, J. Ding, M. Wriedt, J. Nanda, D. Mitlin, *J. Mater. Chem. A* **2017**, *5*, 13511.

[56] N. Patil, C. De La Cruz, D. Ciurduc, A. Mavrandonakis, J. Palma, R. Marcilla, *Adv. Energy Mater.* **2021**, *11*, 2100939.

[57] A. Ciszewski, K. Sron, I. Stepniak, G. Milczarek, *Electrochim. Acta* **2014**, *134*, 355.

[58] J. L. Barton, J. D. Milshtein, J. J. Hinricher, F. R. Brushett, *J. Power Sources* **2018**, *399*, 133.

[59] G. Milczarek, *Electroanalysis* **2007**, *19*, 1411.

[60] X. Ouyang, Y. Deng, Y. Qian, P. Zhang, X. Qiu, *Biomacromolecules* **2011**, *12*, 3313.

[61] Y. Deng, W. Zhang, Y. Wu, Y. Hu, X. Qiu, *J. Phys. Chem. B* **2011**, *115*, 14866.

[62] F. B. D. Santos, P. S. McMichael, A. Whitbeck, A. Jalaee, E. Gyenge, E. J. Foster, *Small* **2024**, *20*, 2309459.

[63] Y. She, X. Li, Y. Zheng, D. Chen, X. Rui, X. Lin, Y. Qin, *Energy Environ. Mater.* **2024**, *7*, e12538.

[64] M. Baloch, M. Alberro, J. Labidi, *Polymers* **2021**, *13*, 643.

[65] F. Fink, F. Emmerling, J. Falkenhagen, *Chem. Methods* **2021**, *1*, 354.

[66] B. Zhou, J. Li, W. Liu, H. Jiang, S. Li, L. Tan, L. Dong, L. She, Z. Wei, *ChemSusChem* **2020**, *13*, 2628.

[67] X. Liu, H. Zhang, Y. Duan, X. Zuan, X. Li, *ACS Appl. Mater. Interfaces* **2020**, *12*, 51573.

[68] Y. Song, X. Li, C. Yan, A. Tang, *J. Power Sources* **2020**, *456*, 228004.

[69] X. Tu, Y. Ma, C. Yang, P. Wang, Z. Gong, N. Sun, Y. Sun, M. Zhou, K. Zhu, *Energy Fuels* **2024**, *38*, 15789.

[70] H. Glatz, E. Tervoort, D. Kundu, *ACS Appl. Mater. Interfaces* **2020**, *12*, 3522.

[71] S. Sun, X. Yang, A. Billings, K. Huang, *Chem. Mater.* **2024**, *36*, 6805.

[72] S. Wu, Y. Chen, T. Jiao, J. Zhou, J. Cheng, B. Liu, S. Yang, K. Zhang, W. Zhang, *Adv. Energy Mater.* **2019**, *9*, 1902915.

[73] L. Qian, H. Zhu, T. Qin, R. Yao, J. Zhao, F. Kang, C. Yang, *Adv. Funct. Mater.* **2023**, *33*, 2301118.

[74] A. Khajeh, Z. Nazari, M. Movahedrad, A. H. Vakili, *Sci. Total Environ.* **2024**, *943*, 173500.

[75] M. Z. Jelyani, S. Rashid-Nadimi, S. Asghari, *J. Solid State Electrochem.* **2017**, *21*, 69.

[76] Z. Chang, D. Henkensmeier, R. Chen, *J. Power Sources* **2019**, *418*, 11.

[77] Z. Chang, D. Henkensmeier, R. Chen, *ChemSusChem* **2017**, *10*, 3193.

[78] H. Fan, J. Zhang, M. Ravivarma, H. Li, B. Hu, J. Lei, Y. Feng, S. Xiong, C. He, J. Gong, T. Gao, J. Song, *ACS Appl. Mater. Interfaces* **2020**, *12*, 43568.

[79] A. Orita, M. G. Verde, M. Sakai, Y. S. Meng, *J. Power Sources* **2016**, *321*, 126.

[80] L.-C. Yu, Y.-C. Luo, W. Feng, S. Zhang, X. Zhang, *J. Mater. Chem. A* **2023**, *11*, 18911.

[81] J. Winsberg, C. Stolze, A. M. Schwenke, S. Muench, M. D. Hager, U. S. Schubert, *ACS Energy Lett.* **2017**, *2*, 411.

[82] Z. Xie, L. Wei, S. Zhong, *Front. Mater. Sci.* **2020**, *14*, 442.

[83] Y. Yao, H. Xu, Z. Tian, J. Zhang, F. Zhan, M. Yan, C. Jia, *ACS Appl. Energy Mater.* **2021**, *4*, 8052.

[84] J. Yu, M. Salla, H. Zhang, Y. Ji, F. Zhang, M. Zhou, Q. Wang, *Energy Storage Mater.* **2020**, *29*, 216.